

Article

Tribological and Thermophysical Properties of Environmentally-Friendly Lubricants Based on Trimethylolpropane Trioleate with Hexagonal Boron Nitride Nanoparticles as an Additive

José M. Liñeira del Río ¹, María J. G. Guimarey ¹, María J. P. Comuñas ¹, Enriqueta R. López ^{1,*} , Jose I. Prado ² , Luis Lugo ²  and Josefa Fernández ¹ 

¹ Laboratory of Thermophysical Properties, NaFoMat Group, Department of Applied Physics, Faculty of Physics, University of Santiago de Compostela, E-15782 Santiago de Compostela, Spain

² Departamento de Física Aplicada, Facultade de Ciencias, Universidade de Vigo, E-36310 Vigo, Spain

* Correspondence: enriqueta.lopez@usc.es

Received: 18 July 2019; Accepted: 7 August 2019; Published: 12 August 2019



Abstract: Dispersions based on hexagonal boron nitride, h-BN, nanoparticles, at 0.50, 0.75 and 1.0 wt.% mass concentrations, in an ester base oil composed mainly of trimethylolpropane trioleate, were investigated as potential nanolubricants. The stability of the dispersions was assessed to determine the reliability of the tribological, thermophysical and rheological measurements. Density and viscosity were measured from 278.15 to 373.15 K, while rheological behavior was analyzed at shear rates from 1 to 1000 s⁻¹ at 283.15 K. Newtonian behavior was exhibited by all nanolubricants at the explored conditions, with the exception of the highest concentration at the lowest shear rates, where possible non-Newtonian behavior was observed. Tribological tests were performed under a normal load of 2.5 N. Wear was evaluated by means of a 3D profiler, scanning electron microscopy and confocal Raman microscopy. The best tribological performance was achieved by the 0.75 wt.% nanolubricant, with reductions of 25% in the friction coefficient, 9% in the scar width, 14% in the scar depth, and 22% of the transversal area, all with respect to the neat oil. It was observed that physical protective tribofilms are created between rubbing surfaces.

Keywords: trimethylolpropane trioleate ester; h-BN nanoparticles; friction; wear; viscosity

1. Introduction

The main role of lubricants is to reduce the friction and wear of moving surfaces, as well as to dissipate heat and remove contamination from the system. Additives are needed in order to improve properties of base lubricants such as oxidation stability, or both anti-friction and anti-wear capabilities. Among the different additives, nanoadditives have the feature of their size enabling them to fill valleys between asperities in the contact area, resulting in a positive lubrication effect and increased heat dissipation [1–3]. Mia et al. [4] recently analyzed environmentally-friendly cooling-lubrication conditions for the production of machine hardened steel in conditions using cutting fluids, concluding that the enhanced heat transfer produced by a cutting lubricant can lead to cleaner production. The use of nanoparticles in the base fluids in the machining processes has become a new trend [5,6].

Boron nitride (BN) nanostructures can be obtained in different morphologies such as nanosheets and spherical nanoparticles. Nanosheets are of particular interest for advanced superlubricity systems [7]. Hexagonal boron nitride, h-BN, has a lamellar crystalline structure in which van der Waals forces exist between sheets, similar to those of graphite and molybdenum disulfide, these being the three compounds which are highly successful solid lubricants [8]. It is precisely these

relatively weak van der Waals interactions between loosely stacked h-BN sheets that provide excellent lubrication characteristics [9]. h-BN, the softest and most lubricious polymorph of BN, has both high thermal stability and thermal conductivity as well as numerous industrial applications, especially in metalworking processes where cleanliness of the working environment is required [10–12]. Additionally, h-BN is an environmentally-friendly material [13], which is being studied as a nanoadditive for liquid lubricants [14–22] because, compared with solid lubricants, liquid lubricant additives present advantages such as faster entrance and replenishment of the sliding interface, and easier removal of wear debris from the contact zone [23].

With respect to the tribological behavior of nanolubricants containing h-BN nanoparticles, Mosleh et al. [14] found that when nanoparticles of h-BN, with irregular flake-like shapes and an average size of 70 nm, were dispersed in commercial sheet metal forming fluids, the friction coefficient for titanium-steel pairs showed little or no improvement; nevertheless, the wear reduction using the 1 wt.% h-BN nanodispersion was 55%. Çelik et al. [15] found that an engine oil (Society of Automotive Engineers (SAE) 10 W) containing h-BN nanoparticles of disk-like shape with an average diameter of 114 nm and thickness of 30–70 nm, led to a 14.4% improvement in the friction coefficient and a 65% decrease in the wear rate with respect to the neat oil for an AISI 4140 steel material. Wan et al. [16] studied nanolubricants composed of a formulated oil 15W-40, a dispersant, and h-BN nanoparticles (disks with average diameter of 120 nm and a single layer thickness of around 30 nm), finding that the nanolubricants with low nanoparticle concentrations significantly improved the anti-friction and anti-wear properties of the base oil. Reeves et al. [17–19] studied the effect of particle size on friction and wear using canola or avocado oils containing nanometer-, submicron-, and micron-sized h-BN particulate additives, finding that the nano-sized particles showed the best tribological performance. Charoo et al. [20] concluded that the use of h-BN nanoparticles (mean size 50 nm) as additives in SAE 20W-50 oil greatly increased the anti-friction and anti-wear properties of the lubricant. Abdullah et al. [21] found that the dispersion of h-BN nanoparticles (70 nm) in a SAE 15W-40 diesel engine oil can lead to an improvement in the extreme pressure lubricating properties as well as in the friction coefficient and wear scar diameter. Bondarev et al. [22] have tested h-BN nanoparticles with different morphologies as additives to PAO6 oil. These authors have found that globular nanoparticles formed by numerous thin h-BN nanosheets (disk-like) noticeably decreased the friction coefficient and significantly reduced the wear rate; however, under applied load, these structures disintegrated into individual nanosheets which could easily be reoriented parallel to the friction direction, thereby minimizing the resistance to shear. Hence, results from the literature show that nano-sized particles, with disk-like or nanosheet morphology, provide better tribological performances as oil additives.

This work aims to evaluate the tribological performance as well as the thermophysical and rheological properties of nanolubricants composed of h-BN nanoparticles (with an average size of 70 nm) dispersed in a synthetic ester oil, mainly composed of trimethylolpropane trioleate (TMPTO). This base oil was chosen because of the following properties: high viscosity index ($VI = 190$), high biodegradability (even higher than 90% in ecological environments), nonflammability, and good lubricity for boundary regimes [24–27]. In this regard, environmental issues and energy savings are encouraging the study of advanced lubricants as substitutes for mineral oils [26]. Furthermore, TMPTO has better oxidative stability and better low-temperature properties than other possible substitutes such as vegetable oils [26]. Due to these properties, TMPTO is extensively used as hydraulic oil, chain oil and metallurgy fluid. In addition, due to its environmentally friendly nature, this oil is a promising alternative to mineral oils and polyalphaolefins (PAOs), not only for these applications, but also in marine and agricultural environments [28,29]. As h-BN is also an eco-friendly material, the resulting nanolubricants can be considered green lubricants. A nanofluid composed of TMPTO [30] and h-BN nanoparticles (with a high thermal conductivity [31]) could also be an excellent cutting fluid [6]. For this work, we have selected h-BN nanoparticles of the lowest commercially available size with disk-like morphology. The tribological study includes measurements of friction coefficients obtained by lubricating a steel/steel contact either with TMPTO (base oil) or with nanolubricants

containing h-BN at 0.50, 0.75 and 1.0 wt.%. Wear was evaluated with a 3D profiler, a scanning electron microscope (SEM), and confocal Raman microscopy. Reductions in the friction coefficients of up to 25% and in the transversal area of up to 22% were found, being the optimum composition 0.75 wt.%. The same trend shown by the friction coefficients was followed by the roughness of the worn surfaces. From confocal Raman microscopy, a protective tribofilm was detected.

2. Materials and Methods

2.1. Materials

The TMPTO sample, kindly provided by Croda (Snaith, UK), belongs to the group of synthetic esters and is composed of 68.3% trimethylolpropane trioleate (TMPTO), 27.6% of a compound with a C=C bond more than TMPTO (i.e., two H atoms less), and 4.1% of a compound with two C=C bonds more than TMPTO (i.e., four H atoms less). The sample used was an aliquot of that used in a previous study [24] where a full characterization was reported. As TMPTO is the major component in the oil, it is referred to as TMPTO in the following sections.

The powder sample of hexagonal boron nitride nanoparticles (h-BN, Chemical Abstracts Service (CAS) Number: 10043-11-5) had a purity of 99.5%, an average particle size of 70 nm, and a specific average area of 19.4 m²/g as indicated by the manufacturer (Iolitec GmbH, Heilbronn, Germany, lot MNC018001). SEM micrographs, using an accelerating voltage of 3 kV, and energy dispersive X-Ray (EDX) analysis of the powders were obtained using a Zeiss Ultraplus field emission scanning electron microscope (FESEM, Carl Zeiss Microscopy GmbH, Jena, Germany). EDX confirmed that the purity of the h-BN powders was approximately 99%. In Figure 1a, a disk-like morphology of the nanoparticles is observed. In addition, nanoparticles were dispersed in n-butanol in order to analyze their possible aggregation. Images were taken with a transmission electronic microscope (TEM) JEOL JEM-2010 (JEOL, Tokyo, Japan), with an accelerating voltage of 200 kV. The TEM image (Figure 1b) shows that some aggregation occurs in this solvent. A non-uniform size distribution of disk-like shaped nanoparticles can be also observed.

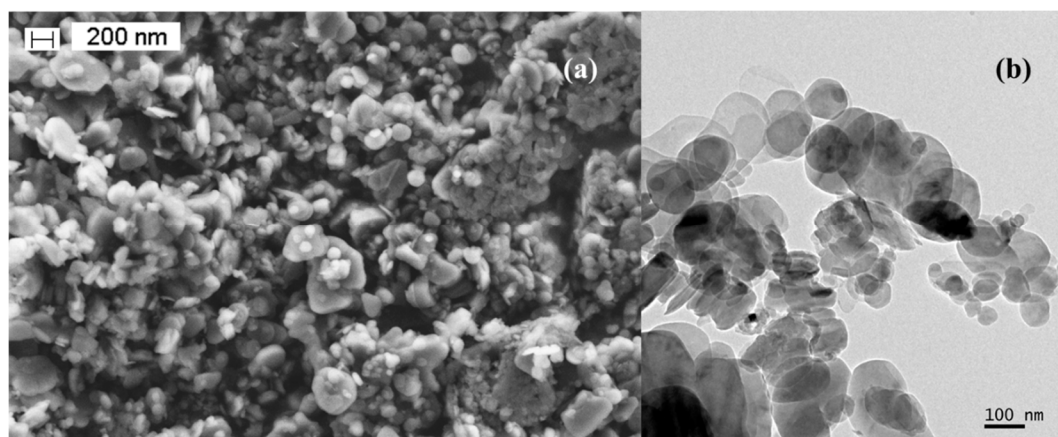


Figure 1. (a) SEM image of the h-BN nanoparticles; (b) TEM image showing h-BN nanoparticles.

Hexagonal boron nitride nanopowders were also characterized by Fourier-transform infrared (FTIR) spectroscopy (Varian, Inc., Palo Alto, CA, USA). The FTIR spectrum (Figure 2) shows two distinct modes at 767.14 and 1324.85 cm⁻¹, both attributed to the *sp*² bonded h-BN according to Aradi et al. [32]. The mode at 767.14 cm⁻¹ represents the A_{1u} out-of-plane bending vibration whereas the mode at 1324.85 cm⁻¹ is the E_{1u} in-plane stretching vibration for h-BN [32–34]. In addition, the Raman spectrum of the h-BN nanopowders (Figure S1) shows the typical mode of hexagonal boron nitride at 1367 cm⁻¹.

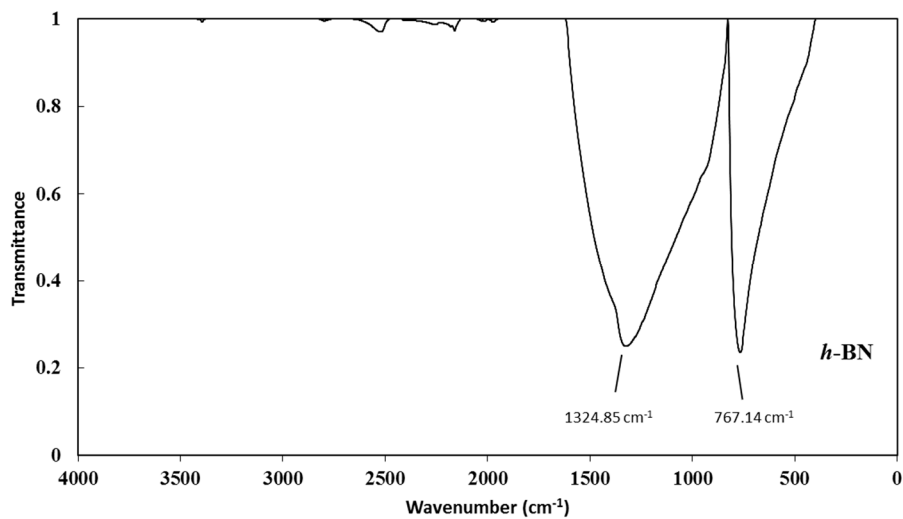


Figure 2. Hexagonal boron nitride FTIR spectrum.

2.2. Preparation of the Nanolubricants

In order to prepare dispersions at different h-BN nanoparticle mass concentrations (0.50, 0.75 and 1.0 wt.%) in the base oil, a multirange Sartorius balance (model MC 210P, Gottingen, Germany, whose readability in the range used is 0.01 mg) was used. The dispersions were sonicated with an ultrasound tip homogenizer Sonopuls HD4200 (Bandelin, Berlin, Germany) for 60 min with an amplitude of 93 μm at 200 W. The dispersions were immersed in an ice-water bath in order to minimize overheating during the sonication process. FTIR spectroscopy can provide valuable information about possible interactions between the constituents of the dispersion. FTIR spectra corresponding to the base oil and to the 0.5 wt.% dispersion of h-BN are plotted in Figure 3. No evidence of formation of new chemical bonds can be concluded from the FTIR profile; furthermore, no peak-shift is reported when h-BN nanoparticles are dispersed into the TMPTO oil. Therefore, this could mean that there are only physical interactions between constituents of the dispersions.

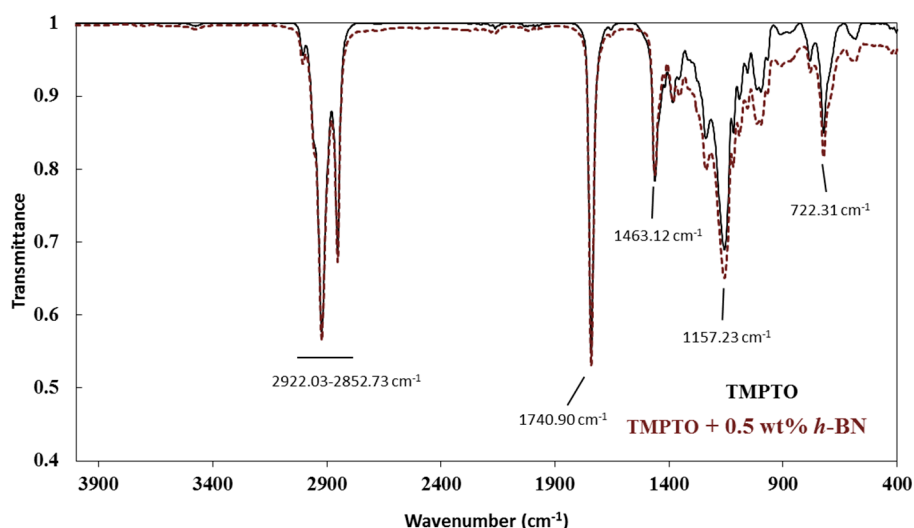


Figure 3. The FTIR spectra: TMPTO (—) and TMPTO + 0.50 wt.% h-BN nanolubricant (-).

In order to check the stability of the dispersions, a visual analysis was carried out for all the prepared nanolubricants. As can be observed in Figure 4, 24 h after their preparation the least and the most concentrated nanodispersions do not show signs of sedimentation. This period is longer than is required to perform the thermophysical, rheological, and tribological studies (around 6 h).

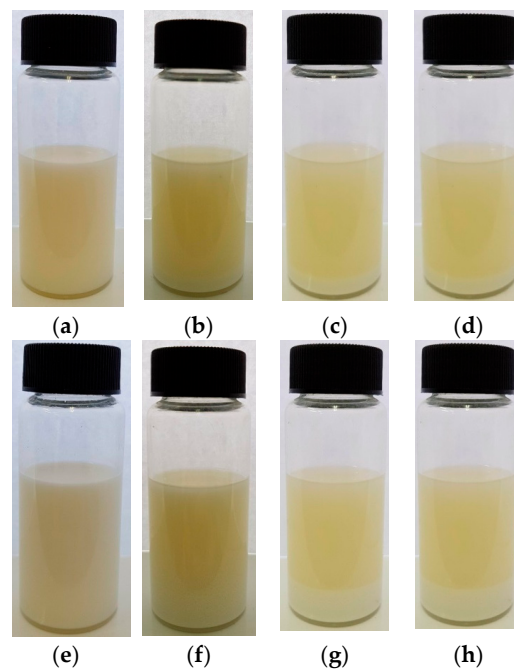


Figure 4. Visual temporal evolution of the dispersions for TMPTO + 0.50 wt.% h-BN: (a) 0 h, (b) 24 h, (c) 48 h, (d) 72 h; and TMPTO + 1.0 wt.% h-BN: (e) 0 h, (f) 24 h, (g) 48 h, (h) 72 h.

To assess the evolution of the average hydrodynamic size of the nanoadditive dispersed in the neat oil, the dynamic light scattering technique (Zetasizer Nano ZS DLS, Malvern Panalytical Ltd, Malvern, UK) was used. This technique provides information about the stability of dispersions even with high nanoparticle concentrations. More details about this technique and the experimental procedure are given elsewhere [24]. After preparation, a sample of each nanolubricant was placed in a measurement cell and rested under static conditions, i.e., without shaking or sonicating. DLS data were obtained for even longer than the tribological, thermophysical, or rheological time analysis; therefore, size distribution measurements were run for 72 h. Figure 5 reveals that the size distribution obtained by DLS is consistent with the microscopy analysis (Figure 1) of the h-BN nanopowder. As can be checked, the shape of the distribution curve is maintained over the studied time even under the most unfavorable conditions, i.e., rested under static conditions. Moreover, the mean size obtained from these curves is only shifted approximately 12 nm, within the expected uncertainty of this technique. Therefore, the assumption of the main conclusions assessed by visual temporal evolution analysis was confirmed by DLS.

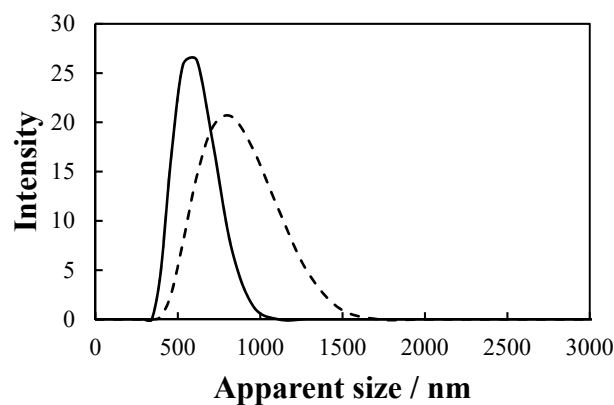


Figure 5. Apparent particle size distributions obtained by DLS for TMPTO + 0.50 wt.% h-BN nanolubricant: 0 h (—) and 72 h (---).

2.3. Thermophysical and Rheological Characterization

The dynamic viscosity and density of the nanolubricants at atmospheric pressure were determined over the temperature range from 278.15 to 373.15 K with a SVM 3000 Anton Paar (Graz, Austria) rotational Stabinger viscometer [35], which includes a vibrating tube densimeter. The device has been described in detail previously [36,37]. The expanded uncertainties ($k = 2$) are 0.02 K for the temperature from 288.15 to 378.15 K and 0.05 K outside this range, $0.0005 \text{ g}\cdot\text{cm}^{-3}$ for density, and 1% in the case of dynamic viscosity. This apparatus has a measurement mode that also allows measurement of the viscosity index according to the ASTM D2270 standard [38]. The rheological behavior of nanodispersions at 283.15 K was analyzed with a rotational rheometer (Physica MCR 101, Anton Paar, GmbH), which has a cone-plate geometry, with a cone diameter of 25 mm and a cone angle of 1° [39,40]. The measurement procedure consists of applying shear stress to the sample and recording the corresponding shear rate. Temperature was controlled during the experiments by a Peltier P-PTD 200 device (Anton Paar, Graz, Austria) with an uncertainty of 0.02 K.

2.4. Tribological Tests

Tribological tests were performed using a tribometer in a ball-on-plate configuration (standard tribometer, CSM Instruments, Peseux, Switzerland, Figure 6) operating in reciprocating mode [41,42]. Chrome steel balls AISI 52100 (diameter: 6 mm, hardness: 803 HV, roughness $< 0.032 \mu\text{m}$) were run against AISI 420 stainless steel plates (40.5 mm \times 21 mm \times 5 mm, hardness: 194 HV) with a mirror finish polishing (roughness, R_a , lower than 11 nm). The type of steel selected for the plate is much softer than the ball, so wear occurs mainly on the plate. AISI 52100 is used in the manufacture of anti-friction bearings, in gears, internal combustion engines, etc. AISI 420 is often used in the automotive sector. Balls and plates were cleaned with a stream of hexane and dried with hot air before the tests. As indicated previously, TMPTO is used as hydraulic oil. Several hydraulic systems have meshing gears as components. The typical maximum Hertzian contact pressure in a gear contact is around 1 GPa. Tests were conducted at room temperature ($\sim 296 \text{ K}$) under a normal load of 2.5 N which corresponds to a maximum contact pressure of 0.88 GPa (mean contact pressure of 0.59 GPa), at a stroke length of 10 mm, maximum speed of $0.10 \text{ m}\cdot\text{s}^{-1}$, and a sliding distance of 500 m. The room humidity was kept close to 50%. The test was started with the CSM Tribotest software (version 4.0). During the test, the software and an inductive displacement transducer enabled recording of the frictional force and the friction coefficient. At least three replicates were run for each concentration.



Figure 6. Tribological experimental setup for reciprocating tests.

In order to analyze the worn surface, after each tribological test the specimens were again rinsed with a stream of hexane for a few seconds. Wear was evaluated in terms of the wear track width

(WTW), wear track depth (WTD), transversal area and roughness, measured with a 3D Optical Profile Sensofar S neox (Terrassa, Spain). Roughness was determined in accordance with the ISO 4287 standard (International Organization for Standardization, Vernier, Switzerland), applying a Gaussian filter with a long wavelength cut-off of 0.25 mm. In addition, scanning electron microscope (SEM) analyses were conducted on the worn surface to examine its morphology. For this purpose, a Carl Zeiss Ultraplus FESEM was used. Information about the composition in the wear track was obtained with confocal Raman microscopy using a WITec alpha300R+ (Ulm, Germany).

On the other hand, the lubrication regime was identified through the dimensionless λ parameter given by:

$$\lambda = \frac{h_{\min}}{R_a} \quad (1)$$

where h_{\min} is the minimum lubricant film thickness given by the Hamrock-Dowson formula for isoviscous-elastic lubrication [43,44]:

$$h_{\min} = 2.8R' \left(\frac{\eta v}{E'R'} \right)^{0.65} \left(\frac{N}{E'R'^2} \right)^{-0.21} \quad (2)$$

where η is the dynamic viscosity of the lubricant, v the sliding velocity, N the normal load, R' the effective contact radius, and E' the effective Young's modulus.

R_a in Equation (1) is the equivalent roughness, given by:

$$R_a = \sqrt{R_{a,1}^2 + R_{a,2}^2} \quad (3)$$

where $R_{a,1}$ and $R_{a,2}$ are the roughness of both contact specimens.

Boundary lubrication occurs when $0.1 < \lambda < 1$, $1 < \lambda < 3$ indicates mixed lubrication, and $\lambda > 3$ designates elastohydrodynamic lubrication [44]. From the mechanical and geometrical properties of both ball and disk, λ values less than 1 were obtained for TMPTO and the nanolubricants; in particular a value of 0.21 was obtained for TMPTO whereas for all the nanodispersions a value of 0.22 was found. Thus, we can conclude that during tribological tests the lubrication regime is boundary.

3. Results and Discussion

3.1. Thermophysical and Rheological Characterization

Densities and viscosities for the nanolubricants are reported in Tables 1 and 2. For the neat oil, these properties have been reported previously [24]. As can be observed in Table 1, for 1 the whole temperature range, density slightly rises when h-BN concentration increases, with densities for the 1 wt.% dispersion being around 0.62% higher than those for TMPTO.

The following empirical equation was used to correlate the density data as a function of both temperature and percentual mass fraction, w , of h-BN in the nanolubricant (ranging from 0 to 1 wt.%).

The parameter values A , B and C , as well as the standard deviation, are reported in Table 3. Equation (4) excellently correlates the experimental values with a standard deviation lower than the experimental uncertainty ($0.005 \text{ g}\cdot\text{cm}^{-3}$).

$$\rho = A + BT + Cw \quad (4)$$

Table 1. Experimental density, $\rho/\text{g}\cdot\text{cm}^{-3}$, of the dispersions TMPTO/h-BN as a function of temperature.

T/K	$\rho/\text{g}\cdot\text{cm}^{-3}$		
	0.50 wt.% h-BN/TMPTO	0.75 wt.% h-BN/TMPTO	1.0 wt.% h-BN/TMPTO
278.15	0.9295	0.9310	0.9318
283.15	0.9263	0.9278	0.9286
288.15	0.9230	0.9245	0.9253
293.15	0.9198	0.9213	0.9221
298.15	0.9166	0.9181	0.9189
303.15	0.9133	0.9148	0.9157
308.15	0.9101	0.9116	0.9124
313.15	0.9068	0.9083	0.9092
318.15	0.9036	0.9051	0.9059
323.15	0.9003	0.9018	0.9027
328.15	0.8970	0.8985	0.8995
333.15	0.8937	0.8952	0.8962
338.15	0.8904	0.8920	0.8929
343.15	0.8872	0.8887	0.8897
348.15	0.8839	0.8854	0.8864
353.15	0.8806	0.8821	0.8831
358.15	0.8773	0.8788	0.8798
363.15	0.8741	0.8756	0.8766
368.15	0.8708	0.8723	0.8733
373.15	0.8676	0.8691	0.8701

Table 2. Experimental dynamic viscosity, $\eta/\text{mPa}\cdot\text{s}$, of the dispersions h-BN/TMPTO as a function of temperature.

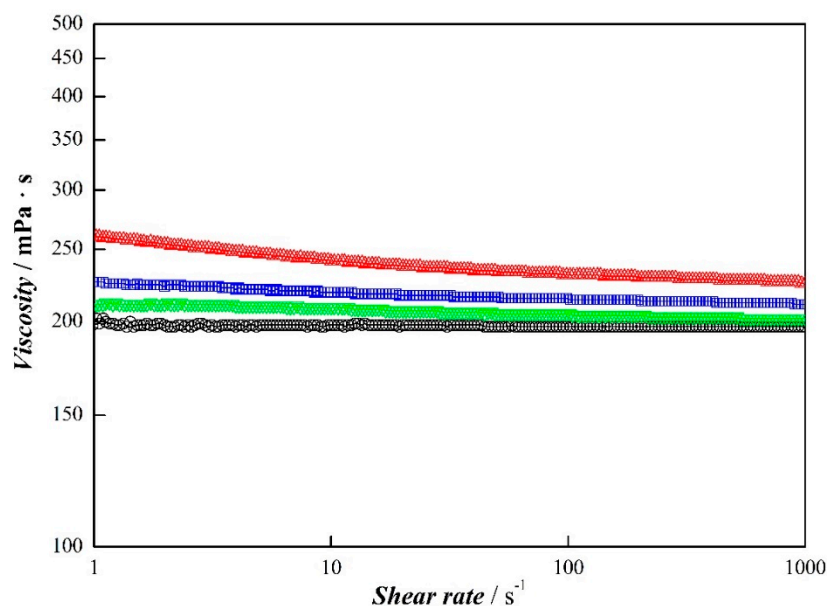
T/K	$\eta/\text{mPa}\cdot\text{s}$		
	0.50 wt.% h-BN/TMPTO	0.75 wt.% h-BN/TMPTO	1.0 wt.% h-BN/TMPTO
278.15	260.5	266.7	263.9
283.15	193.6	198.2	196.5
288.15	147.0	150.5	149.4
293.15	113.6	116.2	115.6
298.15	89.25	91.24	90.88
303.15	71.21	72.76	72.56
308.15	57.63	58.88	58.74
313.15	47.27	48.29	48.20
318.15	39.25	40.11	40.06
323.15	32.96	33.70	33.71
328.15	27.98	28.63	28.69
333.15	23.99	24.56	24.66
338.15	20.74	21.25	21.37
343.15	18.07	18.53	18.67
348.15	15.87	16.29	16.42
353.15	14.03	14.42	14.54
358.15	12.48	12.83	12.93
363.15	11.16	11.48	11.52
368.15	10.04	10.32	10.34
373.15	9.069	9.300	9.352

Table 3. Fitting parameters and standard deviation of the density correlation equation, Equation (4) for h-BN/TMPTO nanolubricants.

Parameter	Value
$A/\text{g}\cdot\text{cm}^{-3}$	1.1079 ± 0.0003
$-10^4 B/\text{g}\cdot\text{cm}^{-3}\cdot\text{K}^{-1}$	6.518 ± 0.009
$10^3 C/\text{g}\cdot\text{cm}^{-3}$	5.65 ± 0.07
$\sigma/\text{g}\cdot\text{cm}^{-3}$	0.0002

On the other hand, the viscosities of the dispersions were higher than those of the base fluid across the whole temperature range (Table 2), with 9.2% being the maximum increase. Nevertheless, the viscosities of the dispersion containing 1 wt.% of h-BN were slightly higher than those of the 0.75 wt.% concentration, for temperatures lower than 323 K (Table 2). However, taking into account the uncertainty (1%), the viscosity values were compatible with the expected viscosity-h-BN load trend. As regards the viscosity index, values of 189.7, 191.7, 193.3 and 194.4 were obtained for the neat oil and the nanolubricants at 0.50, 0.75, and 1.0 wt.% of h-BN, respectively. Thus, this property slightly improved when the load of h-BN nanoparticles increased. This index is an indicator of the viscosity–temperature characteristic of the lubricant.

Moreover, rheological tests for the base oil and the studied dispersions at 283.15 K were carried out with the aim of strengthening the characterization of this key factor in the development of the potential industrial application (Figure 7). As can be observed, the nanolubricants show Newtonian behavior with the exception of 1 wt.% of h-BN at low shear rates, which slightly exhibits a typical shear-thinning behavior with viscosity decreasing with increasing shear rate. The available viscosity data of the Newtonian plateaus for base fluid, 0.50 and 0.75 wt.% nanolubricants agree with those from Table 2 for dispersions and reference [24] for base fluid, with deviations lower than 6.4%, which is within the combined uncertainty.

**Figure 7.** Viscosity, η , as a function of shear rate, $\dot{\gamma}$, for TMPTO nanolubricants at 283.15 K. (○) TMPTO, (▽) 0.50 wt.% in h-BN, (□) 0.75 wt.% in h-BN, and (△) 1.0 wt.% in h-BN.

3.2. Tribological Characterization

The friction coefficients obtained by lubricating the contact with the neat oil or with each of the nanolubricants are shown in Figure 8, as well as in Table 4. As can be observed, the friction coefficients obtained with the dispersions are lower than that corresponding to the neat oil. Reductions of 24%,

25% and 20% of the friction coefficient, μ , were obtained for the concentrations of 0.50, 0.75 and 1.0 wt.%, respectively. Thus, the minimum μ value corresponds to the dispersion with a h-BN content of 0.75 wt.%. Consequently, the addition of h-BN nanoparticles to the base oil clearly improved the anti-friction performance of the neat oil.

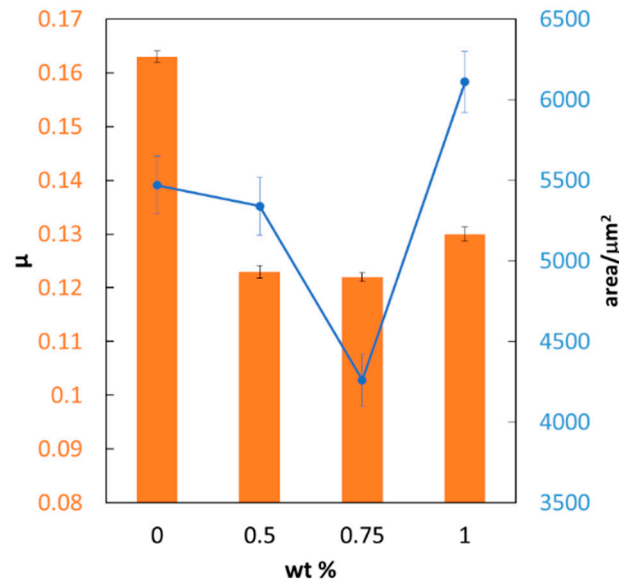


Figure 8. Friction coefficients, μ , (●) and transversal area of the wear track width, area, (■) of TMPTO and the analyzed nanolubricants.

Table 4. Mean values of the friction coefficient, μ , and of the width, WTW, depth, WTD, and transversal area of the wear track (as a maximum) and their respective standard deviations, σ , for the three nanolubricants and TMPTO.

TMPTO + h-BN								
wt.%	μ	σ	WTW/ μm	$\sigma/\mu\text{m}$	WTD/ μm	$\sigma/\mu\text{m}$	Area/ μm^2	$\sigma/\mu\text{m}^2$
0	0.1632	0.0011	579	14	14.02	0.22	5470	180
0.50	0.1234	0.0012	579	18	13.67	0.31	5340	180
0.75	0.1221	0.0008	529	15	12.11	0.19	4260	160
1.0	0.1303	0.0014	611	19	15.12	0.34	6110	190

Wear was evaluated in terms of the maximum width (WTW) and depth (WTD), and the area of the wear tracks, due to the wear scars on the plates which were wave-shaped (Figure 9a,c), indicating the occurrence of plastic flow [24,45]. The average values of these wear parameters are also reported in Table 4. The nanolubricant containing 0.75 wt.% in h-BN reduced the WTW by 9%, the WTD by 14%, and the transversal area by 22% (Figure 8) with respect to the neat oil. As regards the 0.5 wt.% h-BN nanodispersion, small reductions (2%) were obtained for both the WTD and the transversal area. For the highest h-BN concentration, no wear improvements were found. Consequently, the best anti-friction and anti-wear capability was achieved with the 0.75 wt.% composition. It is important to note that decoupling of wear and frictional behavior was also found by Moslesh et al. [14] for h-BN dispersions in commercial sheet metal forming fluids; however, in this case the wear reduction reached up to 55% while that of friction was almost negligible. In Figure 9b,d, we also present the scar obtained in the balls. As can be seen, a smaller track was obtained with the 0.75 wt.% nanolubricant than with the neat oil. Thus, an optimal concentration of 0.75 wt.% was found for both friction and wear. Optimal concentrations were also found for other nanolubricants [24,46–54], including those containing h-BN nanoparticles [16,17]. At lower concentrations, the base oil governs the behavior because the quantity of nanoparticles is not sufficient to prevent wear whereas when the concentration

is too high, the agglomeration allows the creation of new asperities. In relation to the base oil, these new asperities act as a solid lubricant, leading to a friction decrease but with an adverse effect on the roughness of the worn surface.

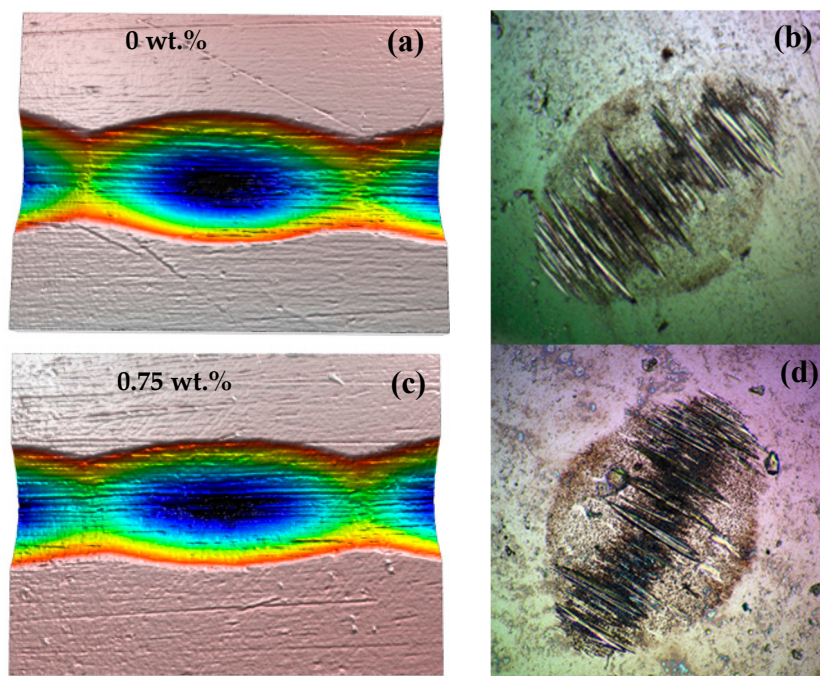


Figure 9. Optical micrographs (10 \times) of a detail of the wear track on the plates (a,c) and the balls (b,d) when the contact was lubricated with TMPTO and with the nanolubricant containing a 0.75 wt.% of h-BN.

Several mechanisms have been proposed to explain the friction reduction and anti-wear properties of nanoparticles in lubricants [1,55] including rolling effect, protective film, mending effect, and polishing effect. The first two mechanisms are due to direct effects of nanoparticles on lubrication enhancement whereas the latter two mechanisms involve a surface enhancement. In addition, the lubricating performance of hexagonal boron nitride can also arise from the easy shearing along the basal plane of its crystalline structure [15]. Rolling effect can be discarded because of the disk-like shape of the h-BN nanoadditives.

In order to analyze the surface enhancements, SEM images of the worn surfaces corresponding to TMPTO and the 0.75 wt.% nanodispersion were taken. As can be observed in Figure 10, a smoother surface was obtained when the contact was lubricated with this nanolubricant instead of with the neat oil. This fact was confirmed by measuring the roughness of the worn surface, R_a , obtained by lubricating the contact with the neat oil and with the different nanolubricants. It is interesting to point out that the same trend found for the friction coefficients, with the h-BN content, was followed by the roughness of the worn surfaces (83, 65, 53, and 71 nm for TMPTO and the 0.5 wt.%, 0.75 wt.% and 1 wt.% h-BN nanolubricants, respectively) Thus, the minimum value of this parameter corresponded to the 0.75 wt.% of h-BN (53 nm). The polishing effect is favored by the shape of h-BN nanoparticles, which results in a smoother worn surface.

Raman spectra on the worn surfaces were recorded with a Raman confocal microscope. Figure 11 shows the results obtained for the surface tested with the nanolubricant containing 0.75 wt.% in h-BN. As can be observed in this figure, the formation of boundary tribofilms containing h-BN (red areas in Figure 11b) is clear, although the signal corresponding to this compound (around 1360–1367 cm^{-1} in Figure 11d) is overlapped with that of the organic carbons of the base oil (in blue). The deconvolution of this spectrum shows the peaks of carbon and h-BN separately (Figure S2). Similar results have been

previously found by Charoo et al. [20] with a SAE 20W-50 oil containing h-BN nanoparticles. These tribofilms decrease the shearing resistance favoring the sliding of both contacting surfaces and could serve as polishing pad to reduce the roughness of the worn surface. In addition, it can be observed that the h-BN nanoparticles are located along several furrows (see Figure S3) on the worn surface; i.e., the mending effect takes place, also resulting in a smoother surface.

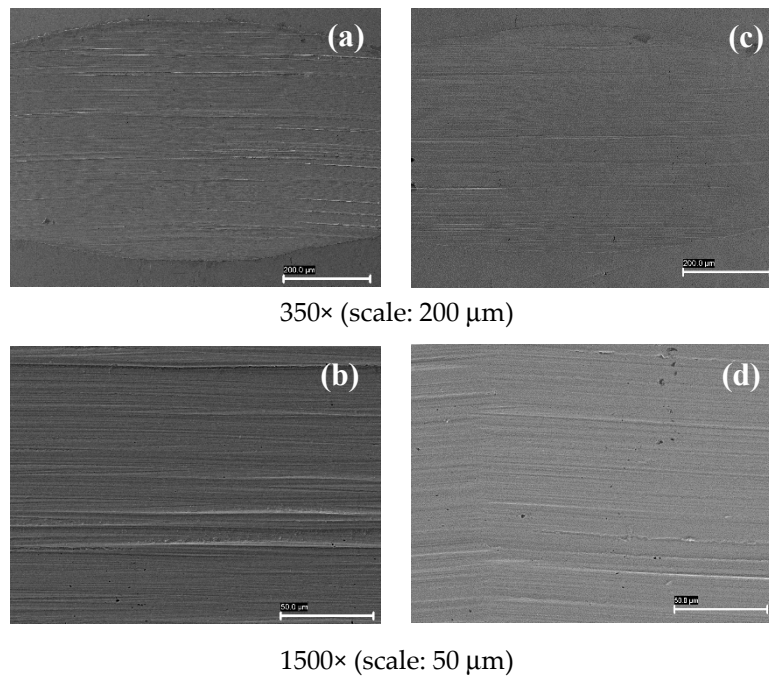


Figure 10. SEM images of the wear scars on the plates lubricated with the neat TMPTO (a,b) and TMPTO + 0.75 wt.% h-BN nanolubricant (c,d).

Figure S4 shows the Raman spectra obtained for the surface tested with the nanolubricant containing 1 wt.% in h-BN in a smaller area (Figure S4a) than in Figure 11a. The presence of h-BN is also detected (green areas in Figure S4b), however, in this case the signal of h-BN (Figure S4d) is detected without overlapping with the signal of organic carbons (Figure S4c). The h-BN additives are deposited and exfoliated at the contact surface through the sliding and shearing actions. It can be pointed out that the size of the areas where h-BN is deposited is in the order of the mean apparent particle size of the aggregates (around 610 nm).

Aggregates are compacted in the contact surface and smeared over the surface. On average, aggregates are larger than the mean roughness in the contact area (see Figure 5). The aggregates actuate as a supporting filling media minimizing the direct contact between the asperities, also lead to sliding friction [56–58] and create a superior protective transfer film [19]. All these mechanisms lead to an overall decrease of friction and wear. However, these larger aggregates could also act as abrasives to increase wear and friction on the rubbing surfaces. Thus, the best anti-wear and anti-friction performance corresponds to the optimal concentration of 0.75 wt.%. For lower concentrations, the number of nanoparticles is insufficient to protect from wear whereas for higher nanoparticle concentrations, the larger presence of agglomerates scratches the surface under loading and results in a wear increase [24]. Binu et al. [59] developed a theoretical method to evaluate the load carrying capacity of journal bearings operating on lubricants containing nanoparticle additives. These authors found that for a journal bearing operating on TiO₂ based nanolubricants, at a constant volume fraction, the load carrying capacity increases with higher nanoparticle aggregate packing ratios. However, aggregation promotes the precipitation of nanoparticles.

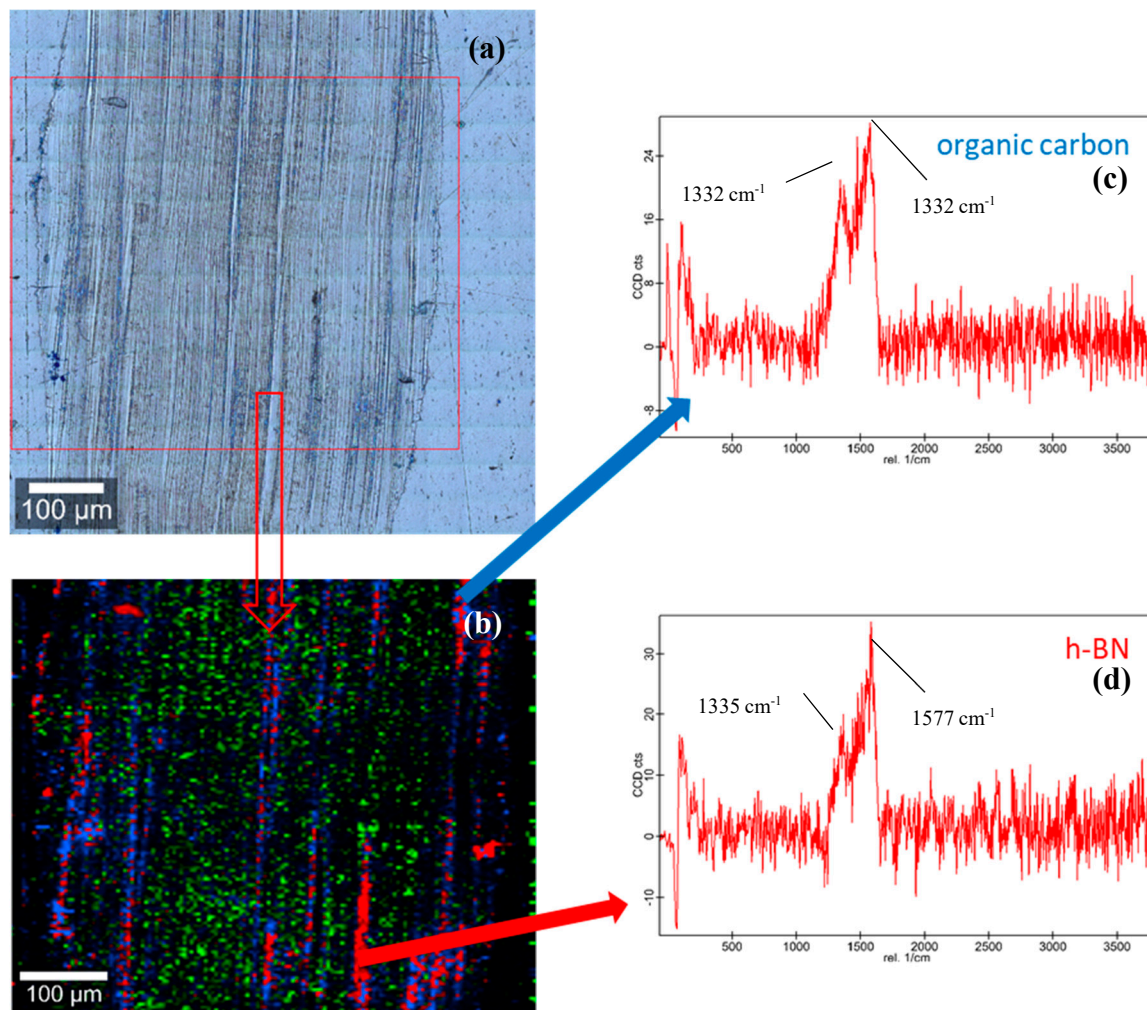


Figure 11. Raman spectra corresponding to the worn surface obtained with the 0.75 wt.% h-BN nanolubricant: (a) Micrograph of the worn surface; (b) Mapping of the components in the worn surface; (c) Spectrum of the blue area; (d) Spectrum of the red area.

4. Conclusions

In this work, dispersions based on TMPTO with 0.50, 0.75 and 1.0 wt.% of h-BN were prepared. Viscosity and density of the nanolubricants were studied by means of a rotational viscometer and a mechanical oscillation densimeter, while a rotational rheometer was employed for rheological characterization. Tribological tests were performed with a CSM standard tribometer under a normal load of 2.5 N, being the contact pair AISI 420/AISI 52100. The following features were achieved:

- Density slightly increased as the concentration of nanoparticles in the nanolubricant increased, up to 0.62%. Density values of the nanolubricants and TMPTO were successfully correlated as a function of both temperature and mass concentrations.
- The viscosity of the nanodispersions was higher than that of the neat oil, with the maximum increase being 9.2%. The nanolubricant with the highest nanoparticle concentration, 1.0 wt.%, showed non-Newtonian behavior at the lowest shear rates at 283.15 K.
- The best anti-friction and anti-wear capability was achieved with the 0.75 wt.% nanolubricant. Thus, reductions of 25% in the friction coefficient, 9% in the case of the wear scar, 14% of the scar depth, and 22% of the transversal area, were obtained with respect to the neat oil.

- h-BN was found by Raman spectroscopy in the worn surfaces tested with the nanolubricants. Polishing, mending and protective tribofilm effects were compatible with the results obtained with SEM, 3D profiler and Raman microscopy, as well as with the morphology of the h-BN nanoparticles.

Supplementary Materials: The following are available online at <http://www.mdpi.com/2079-6412/9/8/509/s1>, Figure S1: Raman spectrum of h-BN nanoparticles, Figure S2: Deconvolution of the Raman spectrum corresponding to the red areas of the mapping (Figure 11d) for the 0.75 wt.% h-BN nanolubricant. Inset: Detail of the overlapping peaks, Figure S3: Optical image of the worn surface tested with the 0.75 wt.% h-BN nanolubricant combined with its Raman spectra mapping (Figure 10), Figure S4: Raman spectra corresponding to the worn surface obtained with the 1 wt.% h-BN nanolubricant.

Author Contributions: The presented work was carried out with the collaboration of all authors. The experimental measurements were performed by J.M.L.d.R., M.J.G.G. and J.I.P. supervised by M.J.P.C., E.R.L., L.L., and J.F. All authors participated in the analysis of the data and discussions and contributed to writing the manuscript. All authors read and approved the final manuscript.

Funding: This work was supported by the Spanish Ministry of Economy and Competitiveness and the ERDF programme through the ENE2014-55489-C2-1/2-R and ENE2017-86425-C2-1/2-R projects. Moreover, this work was funded by the Xunta de Galicia (ED431E 2018/08, GRC ED431C 2016/001 and GRC ED431C 2016-034). These three funders also financed the acquisition of the 3D Optical Profile Sensofar S Neox (UNST15-DE-3156).

Acknowledgments: We would like to thank REPSOL and Croda for providing our laboratory with the TMPTO base oil. The authors are grateful for the use of the RIAIDT-USC analytical facilities, and especially thank Ezequiel Vázquez for his useful advice. Jose I. Prado acknowledges a predoctoral fellowship from the Xunta de Galicia.

Conflicts of Interest: The authors declare no conflicts of interest.

References

1. Gulzar, M.; Masjuki, H.H.; Kalam, M.A.; Varman, M.; Zulkifli, N.W.M.; Mufti, R.A.; Zahid, R. Tribological performance of nanoparticles as lubricating oil additives. *J. Nanopart. Res.* **2016**, *18*, 223. [[CrossRef](#)]
2. Guo, D.; Xie, G.; Luo, J. Mechanical properties of nanoparticles: Basics and applications. *J. Phys. D Appl. Phys.* **2014**, *47*, 013001. [[CrossRef](#)]
3. Shahnazar, S.; Bagheri, S.; Abd Hamid, S.B. Enhancing lubricant properties by nanoparticle additives. *Int. J. Hydrogen Energy* **2016**, *41*, 3153–3170. [[CrossRef](#)]
4. Mia, M.; Gupta, M.K.; Singh, G.; Królczyk, G.; Pimenov, D.Y. An approach to cleaner production for machining hardened steel using different cooling-lubrication conditions. *J. Clean. Prod.* **2018**, *187*, 1069–1081. [[CrossRef](#)]
5. Khan, A.M.; Jamil, M.; Salonitis, K.; Sarfraz, S.; Zhao, W.; He, N.; Mia, M.; Zhao, G. Multi-objective optimization of energy consumption and surface quality in nanofluid sqcl assisted face milling. *Energies* **2019**, *12*, 710. [[CrossRef](#)]
6. Jamil, M.; Khan, A.M.; Hegab, H.; Gong, L.; Mia, M.; Gupta, M.K.; He, N. Effects of hybrid Al₂O₃-CNT nanofluids and cryogenic cooling on machining of Ti-6Al-4V. *Int. J. Adv. Manuf. Technol.* **2019**, *102*, 3895–3909. [[CrossRef](#)]
7. Shtansky, D.V.; Firestein, K.L.; Golberg, D.V. Fabrication and application of BN nanoparticles, nanosheets and their nanohybrids. *Nanoscale* **2018**, *10*, 17477–17493. [[CrossRef](#)]
8. Vuong, T.Q.P.; Liu, S.; Van der Lee, A.; Cuscó, R.; Artús, L.; Michel, T.; Valvin, P.; Edgar, J.H.; Cassabois, G.; Gil, B. Isotope engineering of van der Waals interactions in hexagonal boron nitride. *Nat. Mater.* **2017**, *17*, 152–158. [[CrossRef](#)]
9. Kumari, S.; Sharma, O.P.; Gusain, R.; Mungse, H.P.; Kukrety, A.; Kumar, N.; Sugimura, H.; Khatri, O.P. Alkyl-Chain-Grafted Hexagonal Boron Nitride Nanoplatelets as Oil-Dispersible Additives for Friction and Wear Reduction. *ACS Appl. Mater. Interfaces* **2015**, *7*, 3708–3716. [[CrossRef](#)]
10. Podgornik, B.; Kosec, T.; Kocijan, A.; Donik, Č. Tribological behaviour and lubrication performance of hexagonal boron nitride (h-BN) as a replacement for graphite in aluminium forming. *Tribol. Int.* **2015**, *81*, 267–275. [[CrossRef](#)]
11. Lipp, A.; Schwetz, K.A.; Hunold, K. Hexagonal boron nitride: Fabrication, properties and applications. *J. Eur. Ceram. Soc.* **1989**, *5*, 3–9. [[CrossRef](#)]
12. Shah, F.U.; Glavatskih, S.; Antzutkin, O.N. Boron in tribology: From borates to ionic liquids. *Tribol. Lett.* **2013**, *51*, 281–301. [[CrossRef](#)]

13. Ay, G.M.; Göncü, Y.; Ay, N. Environmentally friendly material: Hexagonal boron nitride. *J. Boron* **2016**, *1*, 66–73.
14. Mosleh, M.; Atnafu, N.D.; Belk, J.H.; Nobles, O.M. Modification of sheet metal forming fluids with dispersed nanoparticles for improved lubrication. *Wear* **2009**, *267*, 1220–1225. [[CrossRef](#)]
15. Çelik, O.N.; Ay, N.; Göncü, Y. Effect of nano hexagonal boron nitride lubricant additives on the friction and wear properties of AISI 4140 steel. *Part. Sci. Technol.* **2013**, *31*, 501–506. [[CrossRef](#)]
16. Wan, Q.; Jin, Y.; Sun, P.; Ding, Y. Tribological behaviour of a lubricant oil containing boron nitride nanoparticles. *Procedia Eng.* **2015**, *102*, 1038–1045. [[CrossRef](#)]
17. Reeves, C.J.; Menezes, P.L.; Lovell, M.R.; Jen, T.-C. The size effect of boron nitride particles on the tribological performance of biolubricants for energy conservation and sustainability. *Tribol. Lett.* **2013**, *51*, 437–452. [[CrossRef](#)]
18. Reeves, C.J.; Menezes, P.L.; Lovell, M.R.; Jen, T.-C. The influence of surface roughness and particulate size on the tribological performance of bio-based multi-functional hybrid lubricants. *Tribol. Int.* **2015**, *88*, 40–55. [[CrossRef](#)]
19. Reeves, C.J.; Menezes, P.L. Evaluation of boron nitride particles on the tribological performance of avocado and canola oil for energy conservation and sustainability. *Int. J. Adv. Manuf. Technol.* **2017**, *89*, 3475–3486. [[CrossRef](#)]
20. Charoo, M.S.; Wani, M.F. Tribological properties of h-BN nanoparticles as lubricant additive on cylinder liner and piston ring. *Lubr. Sci.* **2017**, *29*, 241–254. [[CrossRef](#)]
21. Abdullah, M.I.H.C.; Abdollah, M.F.B.; Tamaldin, N.; Amiruddin, H.; Nuri, N.R.M. Effect of hexagonal boron nitride nanoparticles as an additive on the extreme pressure properties of engine oil. *Ind. Lubr. Tribol.* **2016**, *68*, 441–445. [[CrossRef](#)]
22. Bondarev, A.V.; Kovalskii, A.M.; Firestein, K.L.; Loginov, P.A.; Sidorenko, D.A.; Shvindina, N.V.; Sukhorukova, I.V.; Shtansky, D.V. Hollow spherical and nanosheet-base BN nanoparticles as perspective additives to oil lubricants: Correlation between large-scale friction behavior and in situ TEM compression testing. *Ceram. Int.* **2018**, *44*, 6801–6809. [[CrossRef](#)]
23. Zhang, W.; Cao, Y.; Tian, P.; Guo, F.; Tian, Y.; Zheng, W.; Ji, X.; Liu, J. Soluble, exfoliated two-dimensional nanosheets as excellent aqueous lubricants. *ACS Appl. Mater. Interfaces* **2016**, *8*, 32440–32449. [[CrossRef](#)] [[PubMed](#)]
24. Liñeira del Río, J.M.; Guimarey, M.J.G.; Comuñas, M.J.P.; López, E.R.; Amigo, A.; Fernández, J. Thermophysical and tribological properties of dispersions based on graphene and a trimethylolpropane trioleate oil. *J. Mol. Liq.* **2018**, *268*, 854–866. [[CrossRef](#)]
25. Beran, E.; Łoś, M.; Kmiecik, A. Influence of thermo-oxidative degradation on the biodegradability of lubricant base oils. *J. Synth. Lubr.* **2008**, *25*, 75–83. [[CrossRef](#)]
26. Qiao, S.; Shi, Y.; Wang, X.; Lin, Z.; Jiang, Y. Synthesis of biolubricant trimethylolpropane trioleate and its lubricant base oil properties. *Energy Fuels* **2017**, *31*, 7185–7190. [[CrossRef](#)]
27. Young, A.; Bair, S. Experimental investigation of friction in entrapped elastohydrodynamic contacts. *Tribol. Int.* **2010**, *43*, 1615–1619. [[CrossRef](#)]
28. Wu, Y.; Li, W.; Zhang, M.; Wang, X. Improvement of oxidative stability of trimethylolpropane trioleate lubricant. *Thermochim. Acta* **2013**, *569*, 112–118. [[CrossRef](#)]
29. Chang, T.S.; Yunus, R.; Rashid, U.; Choong, T.S.Y.; Biak, D.R.A.; Syam, A.M. Palm oil derived trimethylolpropane triesters synthetic lubricants and usage in industrial metalworking fluid. *J. Oleo Sci.* **2015**, *64*, 143–151. [[CrossRef](#)]
30. Shashidhara, Y.M.; Jayaram, S.R. Vegetable oils as a potential cutting fluid—An evolution. *Tribol. Int.* **2010**, *43*, 1073–1081. [[CrossRef](#)]
31. Cai, Q.; Scullion, D.; Gan, W.; Falin, A.; Zhang, S.; Watanabe, K.; Taniguchi, T.; Chen, Y.; Santos, E.J.G.; Li, L.H. High thermal conductivity of high-quality monolayer boron nitride and its thermal expansion. *Sci. Adv.* **2019**, *5*, eaav0129. [[CrossRef](#)] [[PubMed](#)]
32. Aradi, E.; Naidoo, S.R.; Billing, D.G.; Wamwangi, D.; Motochi, I.; Derry, T.E. Ion beam modification of the structure and properties of hexagonal boron nitride: An infrared and X-ray diffraction study. *Nucl. Instrum. Methods Phys. Res. B* **2014**, *331*, 140–143. [[CrossRef](#)]

33. Pillari, L.K.; Umasankar, V.; Elamathi, P.; Chandrasekar, G. Synthesis and characterization of nano hexagonal boron nitride powder and evaluating the influence on aluminium alloy matrix. *Mater. Today Proc.* **2016**, *3*, 2018–2026. [[CrossRef](#)]
34. Fakrach, B.; Rahmani, A.; Chadli, H.; Sbai, K.; Bentaleb, M.; Bantignies, J.-L.; Sauvajol, J.-L. Infrared spectrum of single-walled boron nitride nanotubes. *Phys. Rev. B* **2012**, *85*, 115437. [[CrossRef](#)]
35. Novotny-Farkas, F.; Böhme, W.; Stabinger, H.; Belitsch, W. *The Stabinger Viscometer a New and Unique Instrument for Oil Service Laboratories*; World Tribology Congress II; Anton Paar: Vienna, Austria, 2001.
36. Paredes, X.; Fandiño, O.; Comuñas, M.J.P.; Pensado, A.S.; Fernández, J. Study of the effects of pressure on the viscosity and density of diisodecyl phthalate. *J. Chem. Thermodyn.* **2009**, *41*, 1007–1015. [[CrossRef](#)]
37. Gaciño, F.M.; Regueira, T.; Lugo, L.; Comuñas, M.J.P.; Fernández, J. Influence of molecular structure on densities and viscosities of several ionic liquids. *J. Chem. Eng. Data* **2011**, *56*, 4984–4999. [[CrossRef](#)]
38. *ASTM D2270 Standard Practice for Calculating Viscosity Index from Kinematic Viscosity at 40 and 100 °C*; ASTM International: West Conshohocken, PA, USA, 2016.
39. Cabaleiro, D.; Pastoriza-Gallego, M.J.; Gracia-Fernández, C.; Piñeiro, M.M.; Lugo, L. Rheological and volumetric properties of TiO₂-ethylene glycol nanofluids. *Nanoscale Res. Lett.* **2013**, *8*, 286. [[CrossRef](#)] [[PubMed](#)]
40. Cabaleiro, D.; Pastoriza-Gallego, M.J.; Piñeiro, M.M.; Lugo, L. Characterization and measurements of thermal conductivity, density and rheological properties of zinc oxide nanoparticles dispersed in (ethane-1,2-diol+water) mixture. *J. Chem. Thermodyn.* **2013**, *58*, 405–415. [[CrossRef](#)]
41. Otero, I.; López, E.R.; Reichelt, M.; Fernández, J. Friction and anti-wear properties of two tris (pentafluoroethyl) trifluorophosphate ionic liquids as neat lubricants. *Tribol. Int.* **2014**, *70*, 104–111. [[CrossRef](#)]
42. Nair, R.P.; Griffin, D.; Randall, N.X. The use of the pin-on-disk tribology test method to study three unique industrial applications. *Wear* **2009**, *267*, 823–827. [[CrossRef](#)]
43. Ren, S.; Huang, J.; Cui, M.; Pu, J.; Wang, L. Improved adaptability of polyaryl-ether-ether-ketone with texture pattern and graphite-like carbon film for bio-tribological applications. *Appl. Surf. Sci.* **2017**, *400*, 24–37. [[CrossRef](#)]
44. Xie, H.; Jiang, B.; Hu, X.; Peng, C.; Guo, H.; Pan, F. Synergistic Effect of MoS₂ and SiO₂ nanoparticles as lubricant additives for magnesium alloy–steel contacts. *Nanomaterials* **2017**, *7*, 154. [[CrossRef](#)]
45. Plint, G. The Sliding Hertzian Point Contact in Tribotesting: Understanding its Limitations as a Model of Real Systems. In Proceedings of the STLE 70th Annual Meeting and Exhibition, Dallas, TX, USA, 17–21 May 2015.
46. Farsadi, M.; Bagheri, S.; Ismail, N.A. Nanocomposite of functionalized graphene and molybdenum disulfide as friction modifier additive for lubricant. *J. Mol. Liq.* **2017**, *244*, 304–308. [[CrossRef](#)]
47. Guo, Y.-B.; Zhang, S.-W. The Tribological Properties of Multi-Layered Graphene as Additives of PAO2 oil in steel–steel contacts. *Lubricants* **2016**, *4*, 30. [[CrossRef](#)]
48. Gupta, B.; Kumar, N.; Panda, K.; Dash, S.; Tyagi, A.K. Energy efficient reduced graphene oxide additives: Mechanism of effective lubrication and antiwear properties. *Sci. Rep.* **2016**, *6*, 18372. [[CrossRef](#)]
49. Kiu, S.S.K.; Yusup, S.; Chok, V.S.; Taufiq, A.; Kamil, R.N.M.; Syahrullail, S.; Chin, B.L.F. Comparison on tribological properties of vegetable oil upon addition of carbon based nanoparticles. *Mater. Sci. Eng.* **2017**, *206*, 012043. [[CrossRef](#)]
50. Liu, L.; Fang, Z.; Gu, A.; Guo, Z. Lubrication effect of the paraffin oil filled with functionalized multiwalled carbon nanotubes for bismaleimide resin. *Tribol. Lett.* **2011**, *42*, 59–65. [[CrossRef](#)]
51. Liu, Z.; Wei, H.; Tang, B.; Xu, S.; Shufen, Z. Novel light-driven CF/PEG/SiO₂ composite phase change materials with high thermal conductivity. *Sol. Energy Mater. Sol. Cells* **2018**, *174*, 538–544. [[CrossRef](#)]
52. Wu, L.; Gu, L.; Xie, Z.; Zhang, C.; Song, B. Improved tribological properties of Si₃N₄/GCr15 sliding pairs with few layer graphene as oil additives. *Ceram. Int.* **2017**, *43*, 14218–14224. [[CrossRef](#)]
53. Zin, V.; Barison, S.; Agresti, F.; Colla, L.; Pagura, C.; Fabrizio, M. Improved tribological and thermal properties of lubricants by graphene based nano-additives. *RSC Adv.* **2016**, *6*, 59477–59486. [[CrossRef](#)]
54. Liñeira del Río, J.M.; López, E.R.; Fernández, J.; García, F. Tribological properties of dispersions based on reduced graphene oxide sheets and trimethylolpropane trioleate or PAO 40 oils. *J. Mol. Liq.* **2019**, *274*, 568–576. [[CrossRef](#)]
55. Tang, Z.; Li, S. A review of recent developments of friction modifiers for liquid lubricants (2007–present). *Curr. Opin. Solid State Mater. Sci.* **2014**, *18*, 119–139. [[CrossRef](#)]

56. Ali, M.K.A.; Xianjun, H.; Essa, F.A.; Abdelkareem, M.A.A.; Elagouz, A.; Sharshir, S.W. Friction and wear reduction mechanisms of the reciprocating contact interfaces using nanolubricant under different loads and speeds. *J. Tribol.* **2018**, *140*, 051606.
57. Lv, J.; Bai, M.; Cui, W.; Li, X. The molecular dynamic simulation on impact and friction characters of nanofluids with many nanoparticles system. *Nanoscale Res. Lett.* **2011**, *6*, 200. [[CrossRef](#)]
58. Kogovšek, J.; Remškar, M.; Mrzel, A.; Kalin, M. Influence of surface roughness and running-in on the lubrication of steel surfaces with oil containing MoS₂ nanotubes in all lubrication regimes. *Tribol. Int.* **2013**, *61*, 40–47. [[CrossRef](#)]
59. Binu, K.G.; Shenoy, B.S.; Rao, D.; Pai, R. A variable viscosity approach for the evaluation of load carrying capacity of oil lubricated journal bearing with TiO₂ nanoparticles as lubricant additives. *Procedia Mater. Sci.* **2014**, *6*, 1051–1067. [[CrossRef](#)]



© 2019 by the authors. Licensee MDPI, Basel, Switzerland. This article is an open access article distributed under the terms and conditions of the Creative Commons Attribution (CC BY) license (<http://creativecommons.org/licenses/by/4.0/>).